High Frequency Scattering by a Thin Lossless Dielectric Slab

WALTER D. BURNSIDE, MEMBER, IEEE, AND KEN W. BURGENER

Abstract—**A high frequency solution for scattering from a thin dielectric slab is developed, based on a modification of the uniform geometrical theory of diffraction solution for a half-plane, with the intention of developing a model for a windshield of a small private aircraft. Results of the theory are compared with experimental measurements and moment method calculations showing good agreement. Application of the solution is also addressed.**

I. INTRODUCTION

THE UNIFORM geometrical theory of diffraction (UTD) has found great success in terms of solving a wide variety of perfectly conducting electromagnetic problems, such as the analysis of patterns for antennas mounted on aircraft [1] and ships [2]. If the horizons of UTD are to be significantly expanded in the future, it is apparent that additional solutions for penetrable bodies need to be developed. One such solution is suggested in this paper for a source in the presence of a three-dimensional thin lossless dielectric slab.

The motivation for this study was prompted in part by recent attempts to develop a general computer code to predict the radiation patterns for antennas mounted on small private aircraft [3]. In that investigation the windshield scattering and not the penetration was frequently found to be a major contributor to the total pattern. However, the perfectly conducting models available for simulating such aircraft structures were found to be completely inadequate for representing the scattering associated with a real-world windshield. Consequently a solution has been developed for a thin lossless dielectric slab. The following sections are a summary of the theoretical developments found in [4] along with some results which demonstrate its validity, plus a discussion of the limitations of the solution.

II. TWO-DIMENSIONAL DIELECTRIC LAYER SCATTERING

Consider the geometry illustrated in Fig. 1 showing a line source radiating in the presence of a thin lossless layer. The layer is composed of a uniform dielectric material subject to the following restrictions. 1) Diffractions may be assumed to emanate from a single point (Q). 2) Energy leaving (Q) tangential to the layer due to a surface wave or transmission through the endface may be ignored. 3) The source is not positioned near the thin layer such that plane wave reflection and transmission coefficients may be applied. The effects of these restrictions on the solution will be examined later.

The total field at an observation point (P) for this problem may be expressed as the sum of the incident, reflected, transmitted, and diffracted fields such that

$$U^{tot} = U^i + U^r + U^t + U^d. \tag{1}$$

Note that U represents the electric field if an electric line source is used, whereas, it represents the magnetic field if a magnetic line source is present.

It is assumed that the individual terms may be expressed in the following forms

$$U^i(P) = \begin{cases} \dfrac{e^{-jks_i}}{\sqrt{s_i}} & \text{regions I and II} \\ 0 & \text{region III,} \end{cases} \tag{2}$$

$$U^r(P) = \begin{cases} R\dfrac{e^{-jks_r}}{\sqrt{s_r}} & \text{region I} \\ 0 & \text{regions II and III,} \end{cases} \tag{3}$$

$$U^t(P) = \begin{cases} 0 & \text{regions I and II} \\ T\dfrac{e^{-jks_i}}{\sqrt{s_i}} & \text{regions III, and} \end{cases} \tag{4}$$

$$U^d(P) = U^i(Q)D\frac{e^{-jks_d}}{\sqrt{s_d}} \quad \text{regions I, II, and III.} \tag{5}$$

Note that throughout this discussion an $e^{j\omega t}$ time dependence is assumed and suppressed. The task now is to derive expressions for the reflection (R), transmission (T), and diffraction (D) coefficients associated with the previous equations using the fundamental postulates of UTD as given in [5].

In order to develop a solution for the reflection coefficient, the following definitions are made. 1) R_1 and R_2 represent

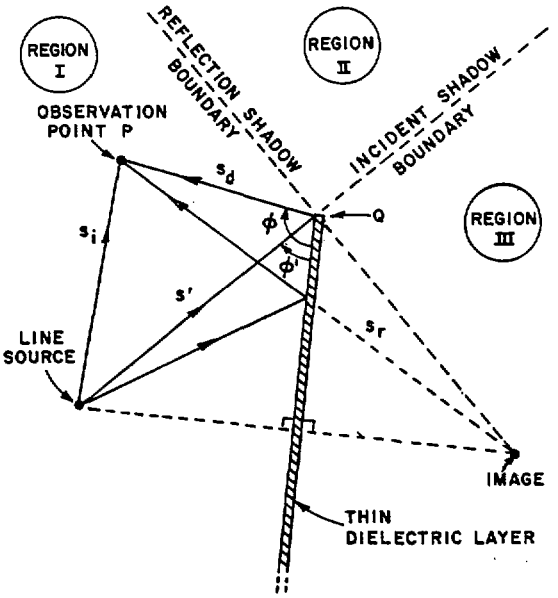

Fig. 1. Thin dielectric layer geometry.

Manuscript received July 1980; revised August 4, 1982. This work was supported in part by NASA/Langley and The Ohio State University Research Foundation under Grant NSG 1498.

W. D. Burnside is with the ElectroScience Laboratory, Department of Electrical Engineering, The Ohio State University, Columbus, OH 43212.

K. W. Burgener was with the ElectroScience Laboratory, Department of Electrical Engineering, The Ohio State University, Columbus, OH. He is now with Campus Crusade for Christ, Los Angeles, CA.

0018-926X/83/0100-0104$1.00

coefficients of single reflection exterior and interior to the layer, respectively. 2) T_1 and T_2 represent transmission coefficients into and out of the layer, respectively. 3) P_d represents the phase delay associated with the field in a single crossing of the layer. 4) P_a represents a term to account for the difference in path length to the observer for different rays leaving the layer in the case of oblique incidence. The plane wave reflection coefficients for a semi-infinite medium interface are determined via continuity of tangential components of the $\vec{E}$ and $\vec{H}$ fields, such that one obtains [6]

$$R_{1(E)} = \frac{\cos\theta_i - \sqrt{\epsilon_r - \sin^2\theta_i}}{\cos\theta_i + \sqrt{\epsilon_r - \sin^2\theta_i}}$$

for the case of an electric line source and

$$R_{1(M)} = \frac{\epsilon_r \cos\theta_i - \sqrt{\epsilon_r - \sin^2\theta_i}}{\epsilon_r \cos\theta_i + \sqrt{\epsilon_r - \sin^2\theta_i}}$$

for the case of a magnetic line source. In both cases one finds that $T_1 = R_1 + 1$, $T_2 = R_2 + 1$, $\theta_r = \theta_i$, and $\sin\theta_t = \sin\theta_i/\sqrt{\epsilon_r}$. Applying the assumption of plane wave incidence and using the geometry illustrated in Fig. 2 one finds that

$$P_d = e^{-jk'l},$$

where $l = d/\cos\theta_t$ and (k) and (k') are the propagation constants in free space and the dielectric medium, respectively. The phase delay associated with each of the reflected field terms illustrated in Fig. 2(b) is given by

$$P_a = e^{jk2l\sin\theta_t\sin\theta_i}.$$

Using the bounce diagram approach illustrated in Fig. 2(a) plus the previous definitions, the total layer reflection coefficient may be expressed in series form by

$$R = R_1 + T_1T_2\sum_{n=2}^{\infty}(R_2)^{2n-3}(P_d)^{2n-2}(P_a)^{n-1}. \tag{6}$$

By recognizing the geometrical series plus that $R_2 = -R_1$ and $T = 1 - R$ for the dielectric layer, (6) reduces to give

$$R_{(M,E)} = \frac{R_{1(M,E)}(1 - P_d^2P_a)}{1 - R_{1(M,E)}^2P_d^2P_a}. \tag{7}$$

Note that one can use (6) for a dielectric-covered ground plane simply by setting $R_{2(E)} = -1$, $R_{2(M)} = 1$, and $T_2 = 0$.

In determining the transmission coefficient a phase factor is given by

$$P_t = e^{jkt},$$

where $t = l\cos(\theta_i - \theta_t)$. Note that P_t is needed to refer the phase to the front face as shown in Fig. 3. The total transmission coefficient is again an infinite sum which reduces to

$$T_{(M,E)} = \frac{(1 - R_{1(M,E)}^2)P_dP_t}{1 - R_{1(M,E)}^2P_d^2P_a}. \tag{8}$$

The geometry for the normal wedge diffraction discussion is depicted in Fig. 1 with the dielectric layer being replaced by a perfectly conducting half-plane. For purposes of this discussion the wedge angle is limited to the half-plane case, which results in

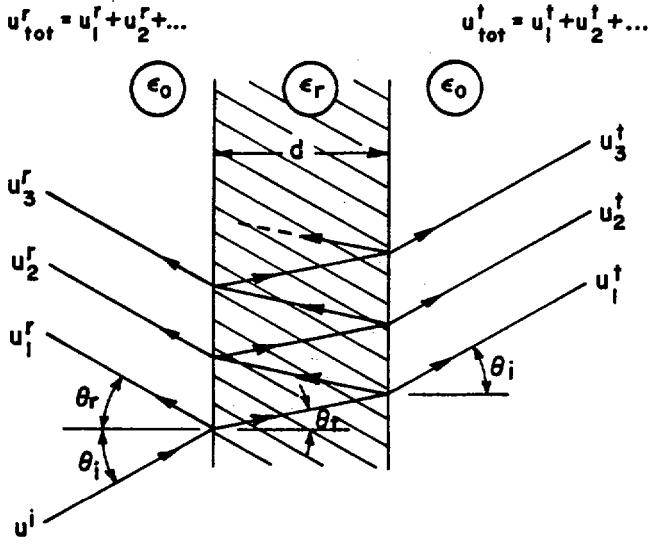

(a)

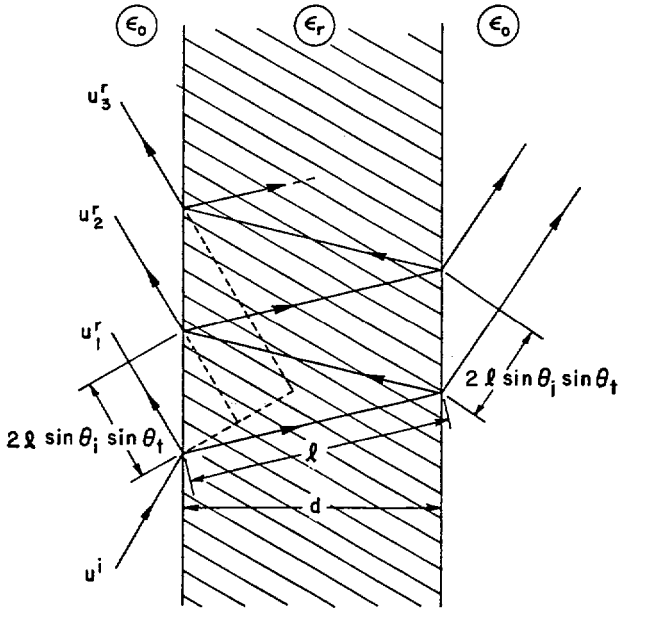

(b)

Fig. 2. (a) Illustration of reflection and transmission for plane-wave incident on thin dielectric layer in free space. (b) Difference in path length to observer for various rays emerging from layer.

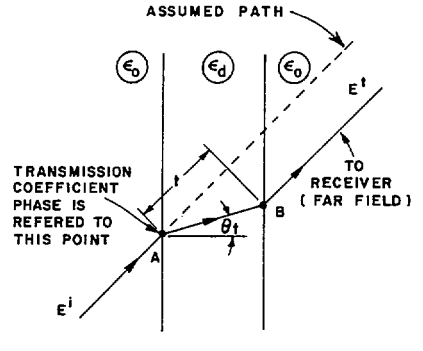

Fig. 3. Transmitted ray phase delay.

a diffraction coefficient given by [5]

$$D_{(M,E)}(\phi,\phi') = \frac{-e^{-j\pi/4}}{2\sqrt{2\pi k}} \cdot \left\{ \frac{F[kLa(\phi-\phi')]}{\cos\left(\frac{\phi-\phi'}{2}\right)} \pm \frac{F[kLa(\phi+\phi')]}{\cos\left(\frac{\phi+\phi'}{2}\right)} \right\} \tag{9}$$

where

$$L = \frac{s's_d}{s'+s_d}, \quad a(\beta) = 2\cos^2(\beta/2),$$

and

$$F(X) = 2j\sqrt{X}e^{jX}\int_{\sqrt{X}}^{\infty} e^{-j\tau^2}\,d\tau.$$

However, one often uses the notation given by

$$D_{(M,E)}(\phi,\phi') = D(\phi-\phi') \pm D(\phi+\phi') \tag{10}$$

with

$$D(\phi \mp \phi') = \frac{-e^{-j\pi/4}}{2\sqrt{2\pi k}} \frac{F[kLa(\phi \mp \phi')]}{\cos\left(\frac{\phi \mp \phi}{2}\right)}. \tag{11}$$

This form shows explicitly how the UTD diffraction coefficients compensate for each of the two discontinuities in the geometrical optics (GO) solution. The $D(\phi-\phi')$ term is associated with the incident shadow boundary, whereas, the $D(\phi+\phi')$ term is associated with the reflection shadow boundary.

Note that in the application of (10) one would use the minus sign for the case of an electric line source and the plus sign for the case of a magnetic line source. Thus R in (3) may be incorporated here, in which case the diffracted field can be written as

$$U^d(P) = U^i(Q)[D(\phi-\phi') + RD(\phi+\phi')]\frac{e^{-jks_d}}{\sqrt{s_d}},$$

with $R = \mp 1$ depending on the polarization.

Let us examine the properties of the diffracted field around the incident shadow boundary such that one finds

$$\text{incident field} = \begin{cases} U^i(P) & \text{lit side, and} \\ 0 & \text{shadow side,} \end{cases}$$

whereas the discontinuous diffraction term is given by

$$U^i(Q)D(\phi-\phi')\frac{e^{-jks_d}}{\sqrt{s_d}} = \begin{cases} -1/2U^i(P) & \text{lit side, and} \\ 1/2U^i(P) & \text{shadow side.} \end{cases}$$

If a thin dielectric layer is considered, then the discontinuity at the incident shadow boundary for the GO terms is given by

$$\text{incident + transmitted fields} = \begin{cases} U^i(P) & \text{lit side, and} \\ TU^i(P) & \text{shadow side,} \end{cases}$$

where $U^i(P)$ represents the incident field and $TU^i(P)$ represents the transmitted field. Thus the discontinuity associated with a transparent dielectric layer is given $(1-T)U^i(P)$. This implies that one can modify the diffracted field term using

$$(1-T)U^i(Q)D(\phi-\phi')\frac{e^{-jks_d}}{\sqrt{s_d}} = \begin{cases} -1/2(1-T)U^i(P) & \text{lit side, and} \\ 1/2(1-T)U^i(P) & \text{shadow side.} \end{cases}$$

Note that this diffraction term plus $U^i(P)$ and $TU^i(P)$ will be continuous across the incident shadow boundary. Using the same approach, let us consider the discontinuous diffraction term associated with the reflection shadow boundary. Around this boundary one finds that

$$RU^i(Q)D(\phi+\phi')\frac{e^{-jks_d}}{\sqrt{s_d}} = \begin{cases} -1/2U^r(P) & \text{lit side, and} \\ 1/2U^r(P) & \text{shadow side,} \end{cases}$$

where R is the reflection coefficient associated with the ray reflected from the surface at the edge, and $U^r(P)$ is the reflected field. Therefore it is conjectured that the total diffraction coefficient for a finite dielectric layer is given by

$$D_{(M,E)}(\phi,\phi') = [(1-T)D(\phi-\phi') + RD(\phi+\phi')]. \tag{12}$$

The values of R and T are given by (7) and (8), with θ_i being the angle between the ray incident on the diffracting edge and the normal to the reflecting surface.

Equations (7), (8), and (12), when used in (1)-(5) give the desired solution for the problem shown in Fig. 1. This has been demonstrated experimentally as will be discussed later. However before presenting this confirmation, the theory will be extended to the more general three-dimensional case.

III. THREE-DIMENSIONAL DIELECTRIC SLAB SCATTERING

In expanding the theory of the previous section into three dimensions it is necessary to express the fields in certain coordinate systems, wherein the coefficients of the previous section are valid. For the reflection and transmission problems, the suitable system is the "ray-fixed coordinate system." By defining the fields in terms of components parallel and perpendicular to the ordinary plane of incidence, the plane containing the incident ray and the normal to the reflecting face, one can utilize the previous coefficients as shown below. Letting $\hat{n}$ be the unit vector normal to the slab, $\hat{I}$ the incident unit vector from the source to a point on the slab, and $\hat{R}$ the reflection unit vector from the point of reflection to the observation point, one may define the following:

$$\hat{u}_\perp = \hat{n} \times \hat{I}/|\hat{n} \times \hat{I}|,$$

$$\hat{u}_\parallel^i = \hat{I} \times \hat{u}_\perp,$$

and

$$\hat{u}_\parallel^r = \hat{R} \times \hat{u}_\perp.$$

Note that ($\perp$) and ($\parallel$) indicate vectors perpendicular and parallel, respectively, to the ordinary plane of incidence, the plane containing $\hat{I}$ and $\hat{n}$. These unit vectors form the orthogonal bases for the ray-fixed coordinate system as illustrated in Fig. 4. The field

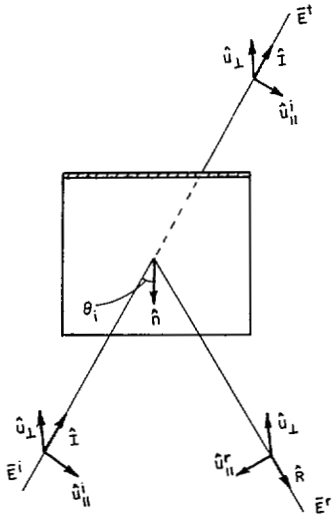

Fig. 4. Ray-fixed coordinate system used for 3D reflection and transmission.

of a ray traveling in the direction of $\hat{I}$ or $\hat{R}$ is now completely specified by its components $E_\perp$ and $E_\parallel$. Note that $E_\perp^i$ corresponds to the two-dimensional (2D) case of an electric line source, and $E_\parallel^i$ corresponds to the 2D case of a magnetic line source. In the ray-fixed system, one may utilize the coefficients of the previous section and express the transmitted and reflected fields in the following manner:

$$\begin{bmatrix} E_\parallel^t \\ E_\perp^t \end{bmatrix} = \begin{bmatrix} T_{(M)} & 0 \\ 0 & T_{(E)} \end{bmatrix} \begin{bmatrix} E_\parallel^i(P) \\ E_\perp^i(P) \end{bmatrix}, \tag{13}$$

and

$$\begin{bmatrix} E_\parallel^r \\ E_\perp^r \end{bmatrix} = \begin{bmatrix} R_{(M)} & 0 \\ 0 & R_{(E)} \end{bmatrix} \begin{bmatrix} E_\parallel^i(Q_r) \\ E_\perp^i(Q_r) \end{bmatrix} f(s^r), \tag{14}$$

where

$$f(s^r) = \sqrt{\frac{\rho_1^r \rho_2^r}{(\rho_1^r + s^r)(\rho_2^r + s^r)}}\, e^{-jks^r}.$$

Note that $E^i(Q_r)$ is the field incident on the point of reflection (Q_r), ρ_1^r and ρ_2^r are equal to the distance from the source to Q_r, and s^r is the distance from Q_r to the receiver (P).

The diffraction coefficients presented in the previous section are valid only when the incident field is expressed by components parallel and perpendicular to the edge-fixed plane of incidence, the plane containing the incident ray and the diffracting edge, and the diffracted field expressed by components parallel and perpendicular to the edge-fixed plane of diffraction, which contains the diffracted ray and the edge. Thus the "edge fixed coordinate system" is introduced and illustrated in Fig. 5. Letting $\hat{e}$ be the unit vector parallel to the diffracting edge, $\hat{I}$ be the incident unit vector from the source to the diffraction point (Q_E), and $\hat{D}$ be the diffraction unit vector from Q_E to the observation point (P), one may define the following:

$$\hat{\phi}' = -\hat{e} \times \hat{I} / |\hat{e} \times \hat{I}|$$

$$\hat{\beta}_0' = \hat{\phi}' \times \hat{I},$$

$$\hat{\phi} = \hat{e} \times \hat{D} / |\hat{e} \times \hat{D}|,$$

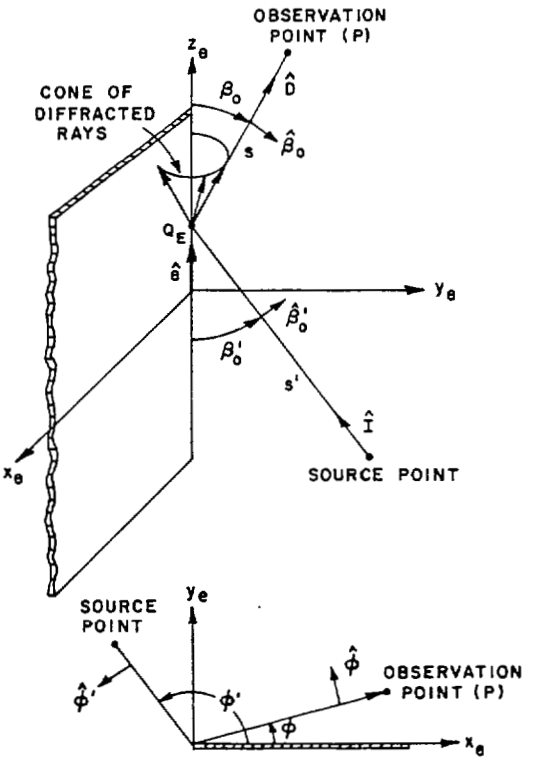

Fig. 5. Edge-fixed coordinate system used for 3D diffraction.

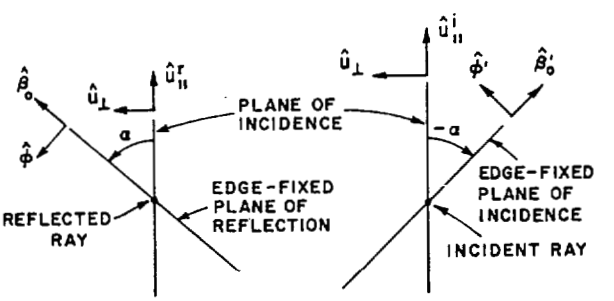

Fig. 6. Comparison of the ray-fixed and edge-fixed coordinate systems. Note that incident and reflected rays along edge shadow boundaries are perpendicular to the page and outward directed.

and

$$\hat{\beta}_0 = \hat{\phi} \times \hat{D}.$$

These vectors form the two orthonormal bases of the edge-fixed coordinate system. Note that the ordinary plane of incidence intersects the edge-fixed plane of incidence along the incident ray, and the edge-fixed plane of diffraction along the diffracted ray. The relationship between these planes, and thus the relationship between the ray-fixed system and edge-fixed system, is depicted in Fig. 6.

It is apparent that the incident field may be expressed in the edge-fixed coordinate system as [7]

$$E_{\beta_0'}^i = E_\parallel^i \cos\alpha - E_\perp^i \sin\alpha, \tag{15a}$$

$$E_{\phi'}^i = E_\parallel^i \sin\alpha + E_\perp^i \cos\alpha. \tag{15b}$$

These expressions may be written more compactly in matrix notation as

$$E_{ef}^i = T(-\alpha) E^i,$$

where

$$T(-\alpha) = \begin{bmatrix} \cos\alpha & -\sin\alpha \\ \sin\alpha & \cos\alpha \end{bmatrix}.$$

Likewise the reflected field is transformed between systems by

$$E^r_{\beta_0} = E^r_{\parallel}\cos\alpha + E^r_{\perp}\sin\alpha$$

$$E^r_{\phi} = -E^r_{\parallel}\sin\alpha + E^r_{\perp}\cos\alpha$$

or

$$E^r_{ef} = T(\alpha)E^r.$$

In a manner similar to that of the previous section, it is assumed that the total diffracted field for a dielectric slab may be expressed as

$$\vec{E}^d = \vec{E}^i(Q_E)[\vec{\vec{A}}D(\phi-\phi') + \vec{\vec{B}}D(\phi+\phi')] \cdot \sqrt{\frac{s'}{s(s'+s)}}\, e^{-jks}, \tag{16}$$

in which the matrices $\vec{\vec{A}}$ and $\vec{\vec{B}}$ serve the same function of scaling the $D(\phi \mp \phi')$ terms to the proper complex value of the discontinuity, as did $(1 - T)$ and (R) previously. To determine the discontinuity one must start with the incident field in the edge-fixed system, transform into the ray-fixed system, perform the operation of reflection or transmission, then transform back into the edge-fixed system. At the reflection boundary one notes that

$$\begin{bmatrix} E^r_{\beta_0} \\ E^r_{\phi} \end{bmatrix} = T(\alpha)\begin{bmatrix} R_{(M)} & 0 \\ 0 & R_{(E)} \end{bmatrix} T^{-1}(-\alpha)\begin{bmatrix} E^i_{\beta_0'} \\ E^i_{\phi'} \end{bmatrix}.$$

Therefore the discontinuity is given by

$$\left\{\begin{bmatrix} \cos\alpha & \sin\alpha \\ -\sin\alpha & \cos\alpha \end{bmatrix}\begin{bmatrix} R_{(M)} & 0 \\ 0 & R_{(E)} \end{bmatrix}\begin{bmatrix} \cos\alpha & \sin\alpha \\ -\sin\alpha & \cos\alpha \end{bmatrix}\begin{bmatrix} E^i_{\beta_0'} \\ E^i_{\phi'} \end{bmatrix}\right\}$$

such that $\vec{\vec{B}}$ is expressed in matrix form by

$$[B] = \left[\begin{array}{c:c} R_{(M)}\cos^2\alpha - R_{(E)}\sin^2\alpha & (R_{(M)}+R_{(E)})\sin\alpha\cos\alpha \\ \hdashline -(R_{(M)}+R_{(E)})\sin\alpha\cos\alpha & -R_{(M)}\sin^2\alpha + R_{(E)}\cos^2\alpha \end{array}\right].$$

Using a similar approach one finds that

$$[A] = \left[\begin{array}{c:c} -1 + T_{(M)}\cos^2\alpha + T_{(E)}\sin^2\alpha & (T_{(M)}-T_{(E)})\sin\alpha\cos\alpha \\ \hdashline (T_{(M)}-T_{(E)})\sin\alpha\cos\alpha & -1 + T_{(M)}\sin^2\alpha + T_{(E)}\cos^2\alpha \end{array}\right].$$

Substituting the previous results for $\vec{\vec{A}}$ and $\vec{\vec{B}}$ into (16), the diffracted field may then be expressed for computational purposes by

$$\begin{bmatrix} E^d_{\beta_0} \\ E^d_{\phi} \end{bmatrix} = \begin{bmatrix} -D_a & -D_b \\ -D_c & -D_d \end{bmatrix}\begin{bmatrix} E^i_{\beta_0'} \\ E^i_{\phi'} \end{bmatrix}\sqrt{\frac{s'}{s(s'+s)}}\, e^{-jks} \tag{17}$$

where

$$D_a = [1 - T_{(M)}\cos^2\alpha - T_{(E)}\sin^2\alpha]D(\phi-\phi') - [R_{(M)}\cos^2\alpha - R_{(E)}\sin^2\alpha]D(\phi+\phi'),$$

$$D_b = [-(T_{(M)}-T_{(E)})\sin\alpha\cos\alpha]D(\phi-\phi') - [(R_{(M)}+R_{(E)})\sin\alpha\cos\alpha]D(\phi+\phi'),$$

$$D_c = [-(T_{(M)}-T_{(E)})\sin\alpha\cos\alpha]D(\phi-\phi') + [(R_{(M)}+R_{(E)})\sin\alpha\cos\alpha]D(\phi+\phi').$$

and

$$D_d = [1 - T_{(M)}\sin^2\alpha - T_{(E)}\cos^2\alpha]D(\phi-\phi') + [R_{(M)}\sin^2\alpha - R_{(E)}\cos^2\alpha]D((\phi+\phi').$$

The previous expressions for the three-dimensional diffraction coefficient are very significant for many reasons. First if a perfectly conducting ground plane were used here, then $T_{(M)} = T_{(E)} = 0$, $R_{(M)} = 1$, and $R_{(E)} = -1$ such that $D_a = D(\phi-\phi') - D(\phi+\phi')$, $D_b = D_c = 0$, and $D_d = D(\phi-\phi') + D(\phi+\phi')$. Note that this result agrees with the perfectly conducting solution of [6]. It is interesting to observe that the dielectric slab diffracts a cross polarized field in that a $\hat{\phi}'$ incident field creates both $\hat{\phi}$ and $\hat{\beta}_0$ components, etc. Second even though this analysis has been directed toward the solutions for thin dielectric slabs, one can apply it to any electromagnetic problem for which the structure is thin and the associated reflection and transmission coefficients are known, either analytically or from experimental data. For example one can use this solution to treat the diffraction from a finite dielectric slab placed on a large ground plane, the diffraction from a finite absorber panel or an absorber panel on a ground plane and the diffraction from a finite metal radome which is terminated into the skin of an aircraft or missile. These are just a few examples that come to mind.

IV. RESULTS

A wide variety of results can be found in [4]; however, some of the more interesting cases are presented here. In the first case, let us consider the two-dimensional dielectric strip problem shown in Fig. 7. A moment method solution has been developed by Richmond [8] for this particular geometry which is used here for comparison purposes. Such a set of pattern comparisons is shown in Fig. 8 for an electric line source positioned various distances above the dielectric strip. Note that the two solutions agree well if the line source is at least a wavelength away from the strip. Another set of results is shown in Fig. 9, where the two solutions are compared as the electric line source is rotated around the dielectric strip at a fixed distance from its center. Even though the line source is positioned rather close to the strip, it appears that good agreement is obtained provided that the line source is not too close to grazing ($|\phi_s| \leqslant 60°$, as illustrated in Fig. 7). In that the surface wave associated with the dielectric strip is neglected in this analysis, it is not surprising that the solution begins to fail for source positions close to grazing.

The second set of results is for a half-wavelength dipole mounted above a square polystyrene covered ground plane as shown in Fig. 10. Various planar pattern cuts are shown in Fig. 11. Note that very good agreement is obtained even for the

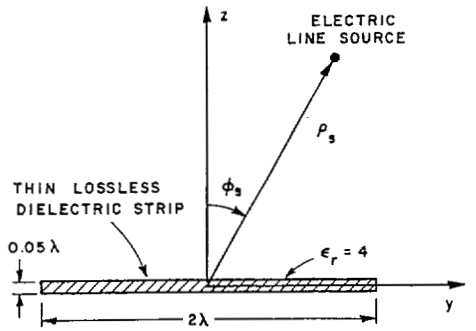

Fig. 7. Geometry used for GTD/MM comparisons. Note λ indicates the free space wavelength.

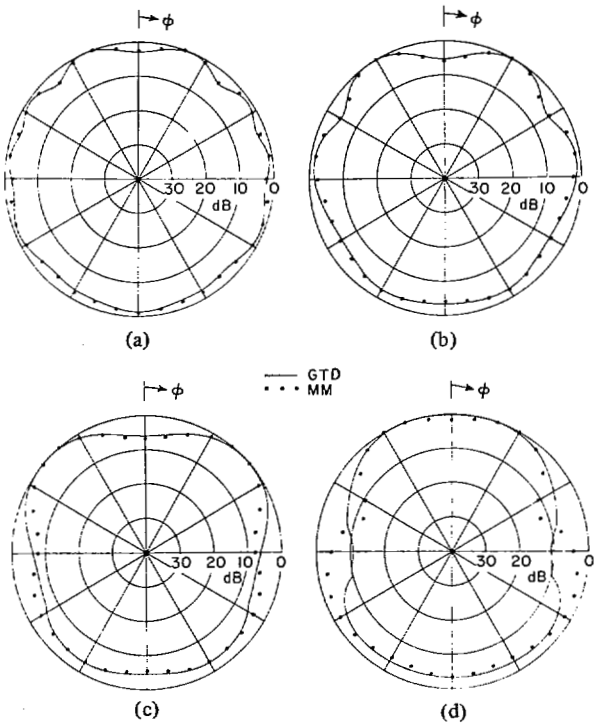

Fig. 8. GTD/MM comparison with electric line source, varying source to slab distance (ρ_s), using geometry shown in Fig. 7 with $\phi_s = 0°$. (a) $\rho_s = 2\lambda$. (b) $\rho_s = \lambda$. (c) $\rho_s = \lambda/2$. (d) $\rho_s = \lambda/4$.

$\phi = 45°$ pattern cut which is taken across the slab corners. In order to achieve this result, a corner diffraction term is also included in the solution using the method suggested by Burnside et al. [9]. In any event it is apparent that the solution developed here is valid, provided the dielectric layer is thin (less than λ/4), the source is at least a wavelength away from the slab, and the source is not positioned close to grazing.

Two examples are used here to indicate the significance of this solution. In order to illustrate the effect of the dielectric layer, a comparison is made between the *E*-plane patterns for the geometry of Fig. 10 with and without the thin dielectric layer, and is shown in Fig. 12. Note that the presence of the dielectric layer causes the pattern peaks to switch to nulls and vice versa. The effect of the diffracted field is illustrated in Fig. 13, where the *E*-plane pattern is computed with and without the diffracted component present. It is apparent from this result that the diffracted field significantly affects the results.

V. CONCLUSION

Studies including those presented here have demonstrated the validity of the modification of the geometrical theory of diffraction (GTD) to include scattering from thin dielectric slabs. The limitations associated with this theory are as follows. 1) The source must be at least a wavelength or so away from the slab in order to assume plane-wave propagation with the slab, 2) the angle between the incident ray and the slab normal must not be much greater than 60° or so in order to avoid exciting a surface wave, and 3) the thickness of the slab must be less than about a quarter wavelength. Within these limits the theory is accurate and the solution is very efficient.

This solution can be extended to treat the diffractions from conducting/dielectric junctions as well as lossy dielectric layers, as will be presented in a future paper.

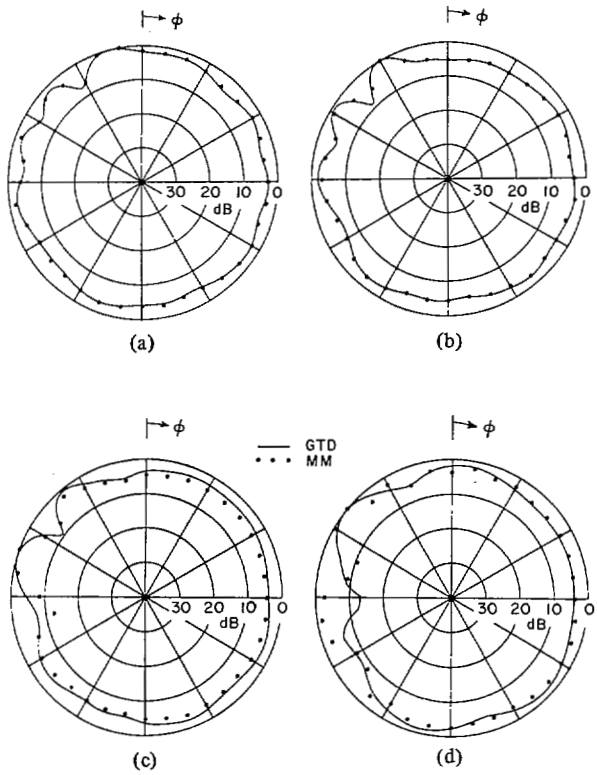

Fig. 9. GTD/MM comparison with electric line source and varying ϕ_s, using the geometry shown in Fig. 7 with $\rho_s = 2\lambda$. (a) $\phi_s = 20°$. (b) $\phi_s = 40°$. (c) $\phi_s = 60°$. (d) $\phi_s = 80°$.

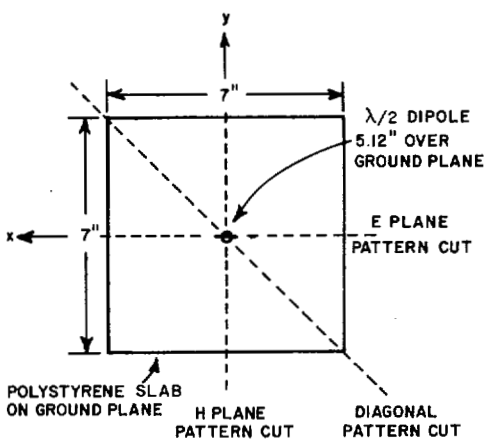

Fig. 10. Polystyrene slab which is 0.2715-in thick and $\epsilon_r = 2.55$ is mounted flush on square ground plane. Structure is illuminated by dipole mounted 5.12-in above center of plate. Using normal spherical coordinates, patterns are measured by varying θ with ϕ constant. Note that *z* axis is into page.

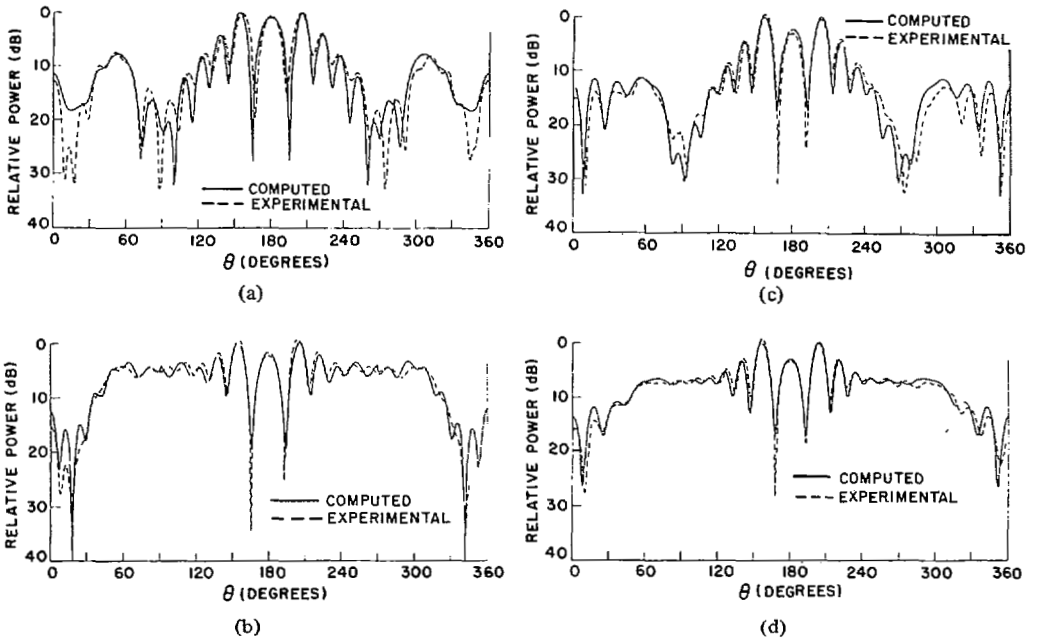

Fig. 11. Patterns for dipole over a polystyrene-covered ground plane at 8 GHz. (a) E-plane pattern ($\phi = 0°$). (b) H-plane pattern ($\phi = 90°$). (c) θ Component for diagonal pattern ($\phi = 45°$). (d) ϕ Component for diagonal pattern ($\phi = 45°$).

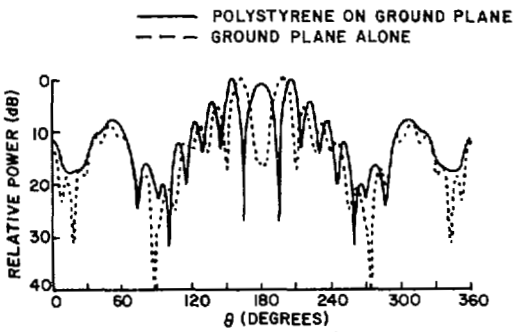

Fig. 12. Comparison of E-plane patterns of geometry illustrated in Fig. 10 with and without the polystyrene slab.

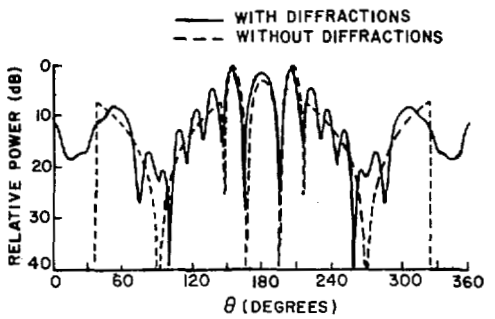

Fig. 13. Comparison of E-plane patterns of geometry illustrated in Fig. 10 with and without diffractions.

REFERENCES

[1] W. D. Burnside, M. C. Gilreath, R. J. Marhefka, and C. L. Yu, "A study of KC-135 aircraft antenna patterns," *IEEE Trans. Antennas Propagat.*, vol. AP-23, no. 3, May 1975.

[2] R. J. Marhefka and W. D. Burnside, "Numerical electromagnetic code (NEC)-base scattering code. Part I: User's manual," Ohio State Univ. ElectroSci. Lab., Dept. Elect. Eng., Rep. 784508-18, Sep. 1979, prepared under Contract N00123-76-C-1371 for Naval Regional Procurement Office.

[3] K. W. Burgener and W. D. Burnside, "Analysis of private aircraft antenna patterns," Ohio State Univ. ElectroSci. Lab., Dept. Elect. Eng., Rep. 710964-2, Jan. 1979, prepared under Grant NSG 1498 for National Aeronautics and Space Administration, Langley Research Center.

[4] K. W. Burgener, "High frequency scattering from a thin lossless dielectric slab," Ohio State Univ. ElectroSci. Lab. Dept. Elect. Eng., Rep. 710964-4, Nov. 1979, prepared under Grant NSG 1498 for National Aeronautics and Space Administration, Langley Research Center.

[5] R. G. Kouyoumjian and P. Pathak, "A uniform geometrical theory of diffraction for an edge in a perfectly conducting surface," *Proc. IEEE*, vol. 62, no. 11, pp. 1448–1461, Nov. 1974.

[6] E. Jordan, *Electromagnetic Waves and Radiating Systems*. Englewood Cliffs, NJ: Prentice-Hall, 1950, pp. 135–141.

[7] R. G. Kouyoumjian and P. H. Pathak, "The dyadic diffraction coefficient for a curved edge," Ohio State Univ. ElectroSci. Lab., Dept. Elect. Eng., Rep. 3001-3, Aug. 1973, prepared under Grant NGR 36-008-144 for NASA, Langley Research Center.

[8] J. H. Richmond, "Scattering by a dielectric cylinder of arbitrary cross section shape, *IEEE Trans. Antennas Propagat.*, vol. AP-28, no. 3, pp. 318–327 May 1980.

[9] W. D. Burnside, N. Wang, and E. L. Pelton, "Near field pattern analysis of airborne antennas," *IEEE Trans. Antennas Propagat.*, vol. AP-28, no. 3, pp. 318–327, May 1980.

Walter D. Burnside (S'69–M'72), for a photograph and biography please see page 622 of the July 1981 issue of this TRANSACTIONS.

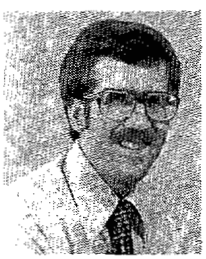

Ken W. Burgener was born in Cleveland, OH on June 7, 1955. He received the B.S. degree in physics from Miami University, Oxford, OH, in 1977 and the M.S. degree in electrical engineering from The Ohio State University, Columbus, in 1979.

From 1977 to 1979 he was associated with the ElectroScience Laboratory, Department of Electrical Engineering, The Ohio State University, where he was a graduate research associate. He is currently working for Campus Crusade for Christ in Los Angeles, CA.